Model Predictive Control Using the Singular Perturbation Theory for Permanent-Magnet Synchronous Machines

Qi Li, Haiming Li, Jianbo Gao, and Ralph Kennel, *Life Senior Member, IEEE*

***Abstract*—This study presents a permanent-magnet synchronous machine (PMSM) model using the singular perturbation theory to obtain the reduced-order model. The fast and slow subsystems of the PMSM drive system are decoupled. The electrical machine's two-time scale property is fully utilized for model predictive control (MPC). An enhanced MPC control strategy is designed to provide dead-beat speed control and improved predictive current control for the external and internal loops. The singular perturbation theory of the PMSM is investigated and assigned to boundary-layer and quasi-steady-state models. The proposed algorithm, built on a dual-core DSP, achieves quick transient dynamics and steady performance. The experimental results confirmed that the proposed method is robust to varying electrical machine parameters and disturbance torque uncertainty.**

***Index Terms*—Electrical drives, model predictive control (MPC), permanent-magnet synchronous machines (PMSMs), singular perturbation theory.**

I. Introduction

FIELD-ORIENTED control (FOC) and direct torque control (DTC) combined with proportional-integral (PI) control in a cascaded scheme are typically current and speed control methods for electrical machines. However, setting the appropriate parameters of the cascaded structure is a prerequisite for stable drive performance.

In the last decades, model predictive control (MPC), which differs from the concept of feedback control, has been thoroughly investigated as an intelligent control approach. MPC enables its application and draws significant interests in power electronics and electrical drives due to the rapid development of microprocessors and more powerful digital microcontrollers with outstanding computing capabilities [1], [2]. MPC naturally provides advantages over FOC and DTC [3], [4], including intuitive principles, affordable calculation, nonlinear constraints, and lower switching frequency [5], [6]. Finite control set model predictive current control (FCS-MPCC) has attracted numerous attentions of many researchers [7], [8], [9], [10] because it ensures desirable current. FCS-MPCC does not need the weighting factor for the dq current track.

Many studies describe the MPC algorithm for the electrical drive, considering both speed and current control. In the conventional MPCC, the PI controller maybe influence the control performance of the whole control system so that several methods can eliminate the PI outer loop in the cascade control structure. The speed control strategy based on MPC in the variable frequency drive systems can be divided into two categories: model predictive direct speed control (MPDSC) [11], [12] and cascaded predictive speed control [13], [14]. FCS-MPC combination with cascaded continuous and finite set MPC (CCF-MPC) is depicted in a cascaded structure of the electrical machine. CCF-MPC enables a tradeoff between the granularity of prediction steps and the prediction horizon length [13]. In [15], a discrete-time state-space model is presented, and the continuous control MPC is implemented on an industrial personal computer to demonstrate the fundamental functionality. In [16], a hierarchical speed and current control framework utilizing MPC in combination with a moving-horizon estimator are presented to guarantee optimal performance control. The autoadaptive discrete-time state-space model with the fuzzy-logic technique is proposed for providing speed control in an induction machine [17]. The proposed discrete-time reduced-order generalized proportional-integral observer reconstructs the virtual system states as well as the lumped disturbances for the output speed prediction [18]. A direct voltage-vector selection-based MPDSC method with a sliding-mode load-torque observer is intended to avoid the weighting factor [19]. An enhanced generalized predictive control (GPC) method is proposed to address the noise and disturbance issues [14]. It demonstrates the GPC is prospective for permanent-magnet synchronous machine (PMSM) drive systems due to its dynamic performance and disturbance rejection capability.

Although the previous methods have obtained some success, there are still some issues that needed to be noticed for the practical application.

1) The appropriate weighting factors in the cost function must be determined and tuned through a large number

Manuscript received 2 June 2023; revised 8 October 2023 and 13 November 2023; accepted 7 December 2023. Date of publication 12 December 2023; date of current version 26 January 2024. This work was supported by Taishan Industrial Leading Talents Project Special Fund. Recommended for publication by Associate Editor L. V. Iyer. *(Corresponding author: Jianbo Gao.)*

Qi Li and Ralph Kennel are with the School of Engineering and Design, Technical University of Munich (TUM), 80333 Munich, Germany (e-mail: qi.li2@tum.de; ralph.kennel@tum.de).

Haiming Li is with the Jining Keli Photoelectronic Industrial Company Ltd., Jining 100124, China (e-mail: lihaiming@sdkeli.com).

Jianbo Gao is with the Shandong Academy of Sciences, Jining 100124, China (e-mail: gaojianbo@sdlaser.cn).

Color versions of one or more figures in this article are available at https://doi.org/10.1109/TPEL.2023.3341455.

Digital Object Identifier 10.1109/TPEL.2023.3341455

of experiments and simulations, which is time consuming and not conducive to future applications.
2) The prior studies are mainly focused on dynamics within the inner current loop, whereas secondary controllers generally act on slowly varying aggregate models that lack current dynamics. Thus, such approaches are insufficient for use in cascaded control strategies with tight coupling at fast time scale.
3) The previous methods predict the long horizon steps of the machine speed. In the practical application, there is a challenge for the microcontroller in which the multivector predictions are adopted to improve the control performance of the whole speed prediction control system. It means the calculation burden is further increased.
4) MPC is vulnerable to model parameter variations owing to temperature and operating pointing variations. These factors have an adverse effect on performance.

Most of the aforementioned research is based on the presumption that the electrical variables have significantly faster dynamics than the mechanical variables, leading to largely required prediction horizons and high computational effort. The conventional control system samples the slow and fast subsystem output values at different sampling frequencies. As such, the fast subsystem evolves on a time scale on which the slow subsystem appears constant. Consistently, assuming that the fast subsystem is converged to a quasi-steady-state value. This traditional analysis leads to missing coupling information between the two-time scale models in the prediction step, affecting the control accuracy. Moreover, the slow subsystem prediction remains holding at the noncoincident sampling period. It also degrades and weakens the dynamic performance of the system. However, this assumption allows us to investigate the electrical and mechanical dynamics separately. Therefore, the MPC's cascaded structure, which inherits the benefits of constructing each control loop independently, is highly promising. We consider a singular perturbation theory to be a natural method for addressing these issues and studying the electrical machine.

The singular perturbation method's multitime scale approach is one of its essential characteristics [20], [21]. The fast and slow subsystems are viewed as two separate subsystems using the singular perturbation theory [20], [22]. When analyzing the dynamic process of the slow subsystem, the fast subsystem's contribution to the slow variable's transition process is disregarded, and the fast subsystem's transitory process is assumed to have terminated and reached its steady state or quasi-steady-state [23]. It is believed that the change of the slow variables can be ignored, and its initial value can be maintained when studying fast variable dynamic processes. The reduced-order model of power-electronic converters in microgrids [24], [25], as well as photovoltaic-powered grid-forming converters [26] is suggested. The proposed configuration takes into account the dynamics and preservation of physical meaning. This is achieved by dividing the system into the fast and slow subsystems via singular perturbation. The utilization of a singular perturbation approach has been found to be an effective method to suppress mechanical resonance in flexible servo systems [27] or joint robots [28]. The stability analysis of the closed-loop system of the PMSM is conducted using the singular perturbation theory and the averaging theorem, as discussed in [29] and [30]. Zhao et al. [31] propose a model-free control scheme for the PMSM through reinforcement learning and singular perturbation.

In this article, the model predictive current control is proposed based on the singular perturbation theory for the high-performance control of the PMSM. In contrast to the existing singular perturbation theory, the proposed method not only enables the prediction of the speed and current horizon and sequences with the reduced-order model in real time but also achieves an optimal model speed track for the PMSM. This control scheme exhibits strong parameter robustness and the capability to reject torque disturbances.

The contributions of the article are briefly summarized as follows.
1) We establish an enhanced MPC control strategy that ensures the design of the dead-beat control for the external speed loop and improved predictive current control for the inner loop separately without weighting factors.
2) The singular perturbation theory is proposed to provide a framework for studying the two-time scale system and decoupling the fast and slow dynamics of the PMSM drive system, which can significantly obtain the reduced-order model. Besides, the reduced-order model has a fast current response and torque disturbance rejection capability.
3) The predictions of both slow and fast models for all the instants are analyzed and improved to get a high-bandwidth speed response. The calculation time of the predictive speed horizon is saved.
4) The application of the singular perturbation theory is employed to assess the robust stability of parameter variations and torque disturbance, which is further validated through experimental analysis conducted under various situations.

The remaining sections of this article are organized as follows. Predictive current and speed control for the singular perturbation model of PMSM drives are proposed. First, the singular perturbation theory is examined to develop quasi-steady-state and boundary-layer models for general control functions, whether linear or nonlinear. The second step is the development of MPC with singular perturbation in two-time scale to optimize sampling and prediction. Third, a detailed explanation the singular perturbation theory in the predictive current control (SPPCC) method based on the PMSM is given. This strategy realizes the proposed SPPCC on dual DSP core. Four experimental tests confirm the effectiveness of the proposed current control strategy.

II. Design of MPC With the Singular Perturbation Theory

A. Singular Perturbation Theory

The singular perturbation theory is applicable to system state equations where the derivatives of state variables depend on a small positive parameter ϵ. The so-called standard singular perturbation model is represented as follows:

$$\dot{\boldsymbol{x}}_1 = f\left(t, \boldsymbol{x}_1, \boldsymbol{x}_2, \epsilon\right) \tag{1}$$

$$\epsilon \dot{\boldsymbol{x}}_2 = g\left(t, \boldsymbol{x}_1, \boldsymbol{x}_2, \epsilon\right) \tag{2}$$

where $t > 0$ is the running time. $\boldsymbol{x}_1 \in \mathbb{R}^{n_1}$ and $\boldsymbol{x}_2 \in \mathbb{R}^{n_2}$ are the state variables of the dynamical system. f and g represent the system state function.

If setting $\epsilon = 0$ abruptly alters the dynamic features of the system, then the differential equation degenerates into an algebraic equation. Consequently, the system's order changes from $n_1 + n_2$ to n_1. The system (2) solution for $\epsilon = 0$ will be represented by $\boldsymbol{x}_{1s}$ and $\boldsymbol{x}_{2s}$. The following equation explains the correlation between $\boldsymbol{x}_{1s}$ and $\boldsymbol{x}_{2s}$:

$$\mathbf{0} = \boldsymbol{g}\left(t, \boldsymbol{x}_{1s}, \boldsymbol{x}_{2s}, \mathbf{0}\right) \Rightarrow \boldsymbol{x}_{2s} = h\left(t, \boldsymbol{x}_{1s}\right). \tag{3}$$

Combining (3) with (1) yields the quasi-steady-state model

$$\dot{\boldsymbol{x}}_{1s} = f\left(t, \boldsymbol{x}_{1s}, h\left(t, \boldsymbol{x}_{1s}\right), \mathbf{0}\right). \tag{4}$$

It is evident that the model (4) describes the system behavior in a slow-time scale. It is thus called slow or the reduced model. The forthcoming analysis will result in a change of coordinates for the dynamical system's fast model

$$\boldsymbol{x}_{2f} = \boldsymbol{x}_2 - h\left(t, \boldsymbol{x}_1\right). \tag{5}$$

The new coordinates $\boldsymbol{x}_{2f} \in \mathbb{R}^{n_2}$ denote the deviation of $\boldsymbol{x}_2$ from its steady-state value $\boldsymbol{h}(t, \boldsymbol{x}_1)$. In the new variables $\boldsymbol{x}_1$ and $\boldsymbol{x}_{2f}$, the new complete singular perturbation model is rewritten as follows:

$$\begin{aligned}
\dot{\boldsymbol{x}}_1 &= f\left(t, \boldsymbol{x}_1, \boldsymbol{x}_{2f} + h\left(t, \boldsymbol{x}_1\right), \epsilon\right) \\
\epsilon \dot{\boldsymbol{x}_{2f}} &= g\left(t, \boldsymbol{x}_1, \boldsymbol{x}_{2f} + h\left(t, \boldsymbol{x}_1\right), \epsilon\right) - \epsilon \frac{\partial h\left(t, \boldsymbol{x}_1\right)}{\partial t} \\
&\quad - \epsilon \frac{\partial h\left(t, \boldsymbol{x}_1\right)}{\partial \boldsymbol{x}_1} f\left(t, \boldsymbol{x}_1, \boldsymbol{x}_{2f} + h\left(t, \boldsymbol{x}_1\right), \epsilon\right).
\end{aligned} \tag{6}$$

Therefore, the quasi-steady-state model (6) can be stated by setting $\boldsymbol{x}_{2f} = 0$. The new time base variable is stretched by $\nu = (t - t_0)/\epsilon$, where t_0 is an initial point time

$$dt = \epsilon d\nu \Rightarrow \epsilon \frac{d\boldsymbol{x}_{2f}}{dt} = \frac{d\boldsymbol{x}_{2f}}{d\nu}. \tag{7}$$

The quasi-steady-state model (6) can be expressed in the ν new time base as

$$\begin{aligned}
\frac{d\boldsymbol{x}_{2f}}{d\nu} &= g\left(t, \boldsymbol{x}_1, \boldsymbol{x}_{2f} + h\left(t, \boldsymbol{x}_1\right), \epsilon\right) - \epsilon \frac{\partial h\left(t, \boldsymbol{x}_1\right)}{\partial t} \\
&\quad - \epsilon \frac{\partial h\left(t, \boldsymbol{x}_1\right)}{\partial x_1} f\left(t, x_1, \boldsymbol{x}_{2f} + h\left(t, \boldsymbol{x}_1\right), \epsilon\right).
\end{aligned} \tag{8}$$

Since in the ν time scale, $t = t_0 + \epsilon\nu$ and $\boldsymbol{x}_1 = \boldsymbol{x}_1(t_0 + \epsilon\nu)$, the variables $\boldsymbol{x}_1$ in (8) exhibit sluggish variation. When $\epsilon = 0$, the variables $\boldsymbol{x}_1(t)$ gradually deviate from their initial values $\boldsymbol{x}_1(t_0)$. It also reduces (8) to the autonomous system

$$\frac{d\boldsymbol{x}_{2f}}{d\nu} = g\left(t_0, \boldsymbol{x}_1\left(t_0\right), \boldsymbol{x}_{2f} + h\left(\boldsymbol{x}_1\left(t_0\right), t_0\right), 0\right). \tag{9}$$

It is assumed that solution $\boldsymbol{x}_{1s}(t)$ is defined for $t \in [0, t_1]$ and $\boldsymbol{x}_{1s} \in D_1 \subset \mathbb{R}^{n_1}$. The autonomous system (9) is then rewritten as

$$\frac{d\boldsymbol{x}_{2f}}{d\nu} = g\left(t, \boldsymbol{x}_1, \boldsymbol{x}_{2f} + h\left(t, \boldsymbol{x}_1\right), 0\right) \tag{10}$$

which is known as the boundary-layer model. For the boundary-layer model's (9) fundamental stability property, the controller design is regarded as the uniform exponential stability of the origin in freezing parameters. The Tikhonov theorem is presented in other literature [21] and is vital for stability. The singular perturbation theory applies not just to linear time-invariant systems but also to linear time-varying and nonlinear systems. It is based on the system time scale features rather than the generic linear or nonlinear characteristics.

B. MPC in Two-Time Scale

After the singular perturbation model has been analyzed, MPC based on the two-time scale features is incorporated into the optimization in Fig. 1. The following assumptions are defined in the MPC algorithm, which takes into account different sampling periods and predictive horizons.

1) $T_s = nT_f$. T_s and T_f are the sampling periods of the slow and fast models, respectively.
2) $P_f \leq T_s/T_f$. P_s is the predictive horizon of the slow model, and P_f is the predictive horizon of the fast model.
3) $U(i) = U(i-1) + \Delta U_f(i) + \Delta U_s(i)$. The control variables of fast and slow models are represented by $U(i)$. $U(i-1)$ is the last instant's state variable. $\Delta U_f(i)$ and $\Delta U_s(i)$ are the control increments of the fast and slow model.

When the sampling instants of the fast and slow models coincide, the system can simultaneously sample the outputs of the fast and slow models. In this case, the control variables calculated from the slow model influences the output of the fast model. Similarly, the control variables computed from the fast model also affects the output of the slow model, so the control response of the system at this instant is the result of the superposition of the control effects from the fast and slow models.

The objective optimization function of the system at the coincident sampling instant is written in the following form:

$$\begin{aligned}
\min J_{\mathrm{s}} &= |Y_s(i) - Y_s^*(i)|^2_{Q_s} + |\Delta U_s(i)|^2_{R_s} \\
&\quad + |Y_f(i) - Y_f^*(i)|^2_{Q_f} + |\Delta U_f(i)|^2_{R_f} \\
Y_s &= \begin{bmatrix} Y_{\mathrm{ss}} \\ Y_{\mathrm{sf}} \end{bmatrix}, \quad \text{and} \quad Y_f = \begin{bmatrix} Y_{\mathrm{fs}} \\ Y_{\mathrm{ff}} \end{bmatrix}
\end{aligned} \tag{11}$$

where Y_s^* and Y_f^* are the reference values of the slow and fast model. Y_{ss} is the predictive sequence values of the slow model at a slow sampling instant. Y_{sf} is the predictive sequence values of the slow model at a fast sampling instant. Y_{fs} is the predictive sequence values of the fast model at a slow sampling instant. Y_{ff} is the predictive sequence values of the fast model at a fast sampling instant. Q_f, R_f, Q_s, and R_s represent weighting factor matrices of dimensions, respectively.

$$Y_{\mathrm{ff}}(i) = \begin{bmatrix} y_{\mathrm{ff}}(i+1|i) \\ y_{\mathrm{ff}}(i+2|i) \\ \vdots \\ y_{\mathrm{ff}}(i+P_f|i) \end{bmatrix}, \; Y_{\mathrm{sf}}(i) = \begin{bmatrix} y_{\mathrm{ff}}(i+1|i) \\ y_{\mathrm{ff}}(i+2|i) \\ \vdots \\ y_{\mathrm{ff}}(i+P_s n|i) \end{bmatrix}$$

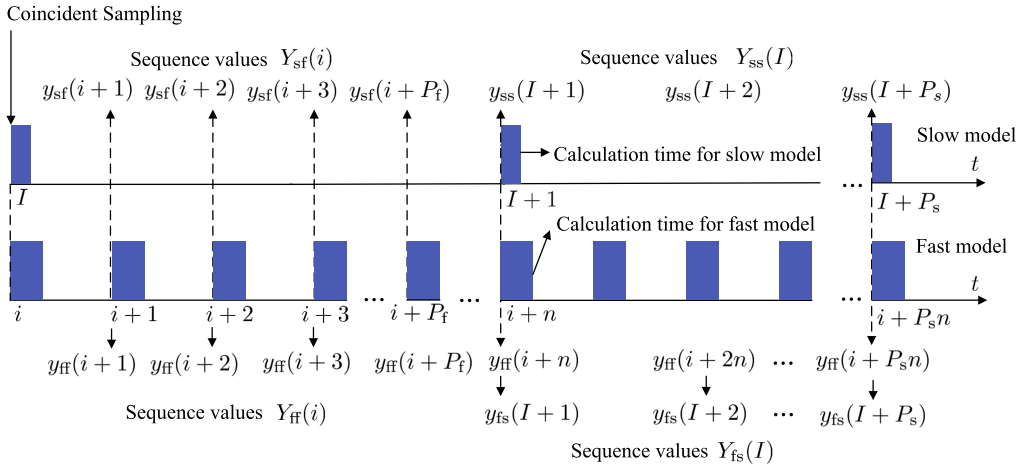

Fig. 1. MPC in two-time scale.

$$Y_{\mathrm{fs}}(I)=\begin{bmatrix} y_{\mathrm{fs}}(I+1|I)\\ y_{\mathrm{fs}}(I+2|I)\\ \vdots\\ y_{\mathrm{fs}}(I+P_f|I)\end{bmatrix}=\begin{bmatrix} y_{\mathrm{fs}}(i+n|i)\\ y_{\mathrm{fs}}(i+2n|i)\\ \vdots\\ y_{\mathrm{fs}}(i+P_fn|i)\end{bmatrix}$$
$$Y_{\mathrm{ss}}(I)=\begin{bmatrix} y_{\mathrm{ss}}(I+1|I)\\ y_{\mathrm{ss}}(I+2|I)\\ \vdots\\ y_{\mathrm{ss}}(I+P_s|I)\end{bmatrix}=\begin{bmatrix} y_{\mathrm{sf}}(i+1|i)\\ y_{\mathrm{sf}}(i+2n|i)\\ \vdots\\ y_{\mathrm{sf}}(i+P_sn|i)\end{bmatrix} \tag{12}$$

where i is the fast sampling instant, and I is the slow sampling instant. When the sampling instants of the fast and slow models do not coincide, the system can only sample the output of the fast model because it is not the sampling instant of the slow model. Consequently, the conventional method can only transmit the output of the fast model at this instant and hold the last slow sampling value of the slow model to predict the sequence value of the system.

For the control in this article, both the slow model's sampling value and the predictive sequence values are utilized. The predictive sequence values for noncoincident sampling instants in (12) are not limited to the fast model. The system's control effect depends on the predictive sequence values of both the fast and slow models.

III. Proposed Arithmetic Model of PMSM Drives

The mathematical model of the PMSM can be described by a well-known set of equations in the synchronously rotating reference coordinates. The stator voltage equations are set as follows:

$$v_d=Ri_d+\dot{\psi}_d-\omega_e\psi_q \tag{13}$$
$$v_q=Ri_q+\dot{\psi}_q+\omega_e\psi_d \tag{14}$$

where v_d, v_q, i_d, and i_q are the dq-axes voltages and currents in the rotating frame, respectively. R is the stator resistance. ω_e is the electrical angular velocity. ψ_d and ψ_q are the stator flux.

$$\psi_d=L_di_d+\psi_f \tag{15}$$
$$\psi_q=L_qi_q \tag{16}$$

where ψ_f is the permanent-magnet flux, and L_d and L_q are the inductance in dq-axes.

The mechanical model of the PMSM can be obtained as follows:

$$T_e=\frac{3}{2}p\left[\psi_fi_q+(L_d-L_q)\,i_di_q\right]=J\dot{\omega}_m+B_r\omega_m+T_L \tag{17}$$

where B_r is the friction constant, J is the inertia constant, and ω_m is the mechanical angular velocity. T_e and T_L are the electrical torque and load torque, respectively.

The stator voltages in the two-level voltage source inverter can be expressed in the stationary and synchronously rotating reference coordinates

$$\begin{bmatrix} v_\alpha\\ v_\beta\end{bmatrix}=\begin{bmatrix} 1 & -\frac{1}{2} & -\frac{1}{2}\\ 0 & \frac{\sqrt{3}}{2} & -\frac{\sqrt{3}}{2}\end{bmatrix}\begin{bmatrix} v_a\\ v_b\\ v_c\end{bmatrix}$$
$$\begin{bmatrix} v_d\\ v_q\end{bmatrix}=\frac{2}{3}\begin{bmatrix} \cos(\theta_e) & \sin(\theta_e)\\ -\sin(\theta_e) & \cos(\theta_e)\end{bmatrix}\begin{bmatrix} v_\alpha\\ v_\beta\end{bmatrix} \tag{18}$$

where v_α and v_β are the voltages in the stator reference frame; and v_a, v_b, and v_c are the phase voltages of the PMSM, respectively. θ_e is the electrical angle.

The d-axis reference current $i_d=0$ for surface-mounted PMSM (SPMSM) is a suitable control strategy. It approximately eliminates the couplings between the speed and current [32]. Meanwhile, neglecting the T_L to reduce the effect of disturbance torque, the electromagnetic torque equation can be simplified to

$$T_e=\frac{3}{2}p\psi_fi_q=K_ti_q=J\dot{\omega}_m+B_r\omega_m \tag{19}$$

where K_t is coefficient of torque.

Through Laplace transformation of (14) and (17), the following results can be obtained:

$$\frac{i_q(s)}{v_q(s)-\omega_e\psi_f}=\frac{1}{sL_q+R}$$

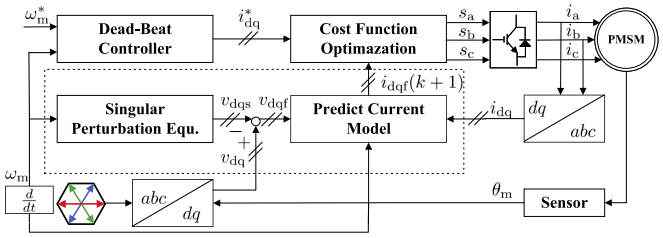

Fig. 2. Schematic structure of the proposed SPPCC for the PMSM drive.

$$\frac{\omega_{\mathrm{m}}(s)}{i_q(s)} = \frac{K_{\mathrm{t}}}{sJ + B_r} \tag{20}$$

where $\omega_e \psi_f$ is back electromotive force (EMF).

The dynamic performance of the SPMSM can be described by two time constants, namely electrical time constant $\frac{L}{R} = \frac{L_q}{R}$ and mechanical time constant $\frac{J}{B_r}$. The electrical time constant is the time required for the current to reach 63.2% of its final value when a zero source impedance stepped input voltage is applied to a machine maintained in its stalled condition.

A. Modeling of the PMSM

Assuming $\epsilon = \frac{L}{R}$ and considering ω_m as the slow variable, and i_d and i_q as the fast variables, the typical singular perturbation model of the PMSM can be shown in Fig. 2, we have

$$\dot{x_1} = A_{11}x_1 + A_{12}x_2 + V_1 \tag{21}$$

$$\epsilon \dot{x_2} = A_{21}x_1 + A_{22}x_2 + B_2 u \tag{22}$$

$$y = \begin{bmatrix} x_1 \\ x_2 \end{bmatrix} \tag{23}$$

where the state vectors are defined as

$$x_1 = \omega_{\mathrm{m}}, \quad x_2 = \left[i_d, i_q\right]^T = \left[i_{\mathrm{ds}} + i_{\mathrm{df}}, i_{qs} + i_{qf}\right]^{\mathrm{T}}$$

$$u = u_{\mathrm{s}} + u_f = \left[v_d, v_q\right]^T = \left[v_{ds} + v_{df}, v_{qs} + v_{qf}\right]^T$$

and $y = \left[\omega_m, i_d, i_q\right]^T$

where the denoted subscript s and f represent variables of slow and fast model, respectively.

And the coefficient matrixes are denoted as follows:

$$A_{11} = -\frac{B_r}{J}, \qquad A_{12} = \left[0, \frac{3p\psi_f}{2J}\right], \quad V_1 = -\frac{T_L}{J}$$

$$A_{21} = \left[0, -\frac{p\psi_f}{R}\right]^T, A_{22} = \begin{bmatrix} -1 & \gamma \\ -\gamma & -1 \end{bmatrix}, B_2 = \frac{1}{R} \tag{24}$$

where $\gamma = \omega_e \frac{L}{R}$ and $\omega_e = p\omega_{\mathrm{m}}$, and p is the rotor pairs of the pole.

When setting $\epsilon = 0$, the standard model of (21) using (3) can be changed into the reduced model as

$$x_2 s = h(x_{1s}, t) = -A_{22}^{-1}\left(A_{21}x_{1s} + B_2 u_{\mathrm{s}}\right)$$

$$\text{and} \quad A_{22}^{-1} = \frac{1}{N}\begin{bmatrix} -1 & -\gamma \\ \gamma & -1 \end{bmatrix} \tag{25}$$

where $u_{\mathrm{s}} = [v_{\mathrm{ds}}, v_{qs}]^T$ and $N = 1 + \gamma^2$.

The quasi-steady state of the PMSM can be obtained in the following expression:

$$\dot{x}_{1s} = A_{\mathrm{s}}x_{\mathrm{s}} + B_{\mathrm{s}}u_{\mathrm{s}} + V_1 \tag{26}$$

where the coefficient matrixes are given as

$$A_{\mathrm{s}} = -\frac{K_{\mathrm{T}}p\psi_f}{JNR} - \frac{B_r}{J}$$

$$\text{and} \quad B_{\mathrm{s}} = \frac{K_{\mathrm{T}}}{JNR}\left[-\gamma, 1\right] \tag{27}$$

where$K_{\mathrm{T}} = \frac{3}{2}p\psi_f$.

The boundary-layer model of the PMSM is expressed as

$$\frac{dx_{2f}}{d\nu} = A_f x_{2f} + B_f u_f, \quad \text{and} \quad d\nu = \frac{dt}{\epsilon} \tag{28}$$

where $x_{2f} = [i_{\mathrm{df}}, i_{qf}]^T$, $A_f = \begin{bmatrix} -1 & \gamma \\ -\gamma & -1 \end{bmatrix}$, and $B_f = \frac{1}{R}$.

B. External Speed Loop as the Slow Model

The dead-beat control is the predictive speed approach to track the speed reference with high bandwidth. The forward Euler approximation is used to implement the speed control. The sampling time T_{s} for the speed loop is ten times larger than the current loop sampling time T_f, $T_{\mathrm{s}} = 10T_f$. Assuming $\omega_{\mathrm{m}}(i+1)$ is equal to the reference value $\omega_{\mathrm{m}}^*(i+1)$ in the next instant, it is possible to solve the q-axis stator current reference as

$$i_q^*(i+1) = A_1 i_q(i) + B_1\omega_{\mathrm{m}}(i) + E_1 T_{\mathrm{L}}(i) + F_1\omega_{\mathrm{m}}^*(i+1) \tag{29}$$

where T_{L} is calculated by torque load observers [14] and the coefficient matrix is

$$A_1 = -1 + \frac{B_r T_{\mathrm{s}}}{J}, \quad B_1 = -\frac{4J}{3T_{\mathrm{s}}p\psi_f} + \frac{4B_r}{3p\psi_f} - \frac{2T_{\mathrm{s}}B_r^2}{3Jp\psi_f}$$

$$E_1 = \frac{4}{3p\psi_f} - \frac{2T_{\mathrm{s}}B_r}{3Jp\psi_f}, \quad \text{and} \quad F_1 = \frac{4J}{3T_{\mathrm{s}}p\psi_f}. \tag{30}$$

C. Internal Current Loop as Fast Model

For the control of the SPMSM, the algorithm of $i_d = 0$ is an alternative choice. The following assumptions are considered:

1) when the d-axis reference current $i_d^* = 0$, $v_{\mathrm{ds}} = 0$ is supposed to happen;
2) un the small-time scale, $i_d = i_{\mathrm{df}}$, and $i_q = i_{qf}$.

Therefore, v_{qs} needs to be calculated from a quasi-steady-state model (26) as

$$v_{qs}(i) = \left(\dot{\omega}_{\mathrm{m}}(i) + \frac{K_{\mathrm{T}}p\psi_f}{JNR} + \frac{B_r}{J}\omega_{\mathrm{m}}(i) + \frac{T_{\mathrm{L}}}{J}\right)\frac{JNR}{K_{\mathrm{T}}} \tag{31}$$

where $\dot{\omega}_{\mathrm{m}}(i) = (\omega_{\mathrm{m}}^*(i+1) - \omega_{\mathrm{m}}(i))/T_{\mathrm{s}}$. Because $w_{\mathrm{m}}^*(i+1)$ is the speed value at the next instant, it easily causes the system to oscillate. It is necessary to add the following equation in Fig. 3:

$$v_{qs} = \begin{cases} \frac{V_{\mathrm{dc}}}{\sqrt{3}} & if \frac{v_{qs}}{\lambda} > \frac{V_{\mathrm{dc}}}{\sqrt{3}} \\ \frac{v_{qs}}{\lambda} & if \frac{|v_{qs}|}{\lambda} \le \frac{V_{\mathrm{dc}}}{\sqrt{3}} \\ -\frac{V_{\mathrm{dc}}}{\sqrt{3}} & if \frac{v_{qs}}{\lambda} < -\frac{V_{\mathrm{dc}}}{\sqrt{3}} \end{cases} \tag{32}$$

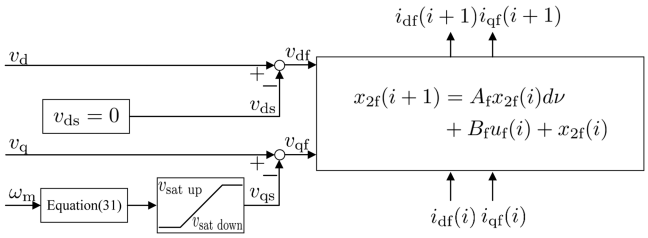

Fig. 3. Block diagram of the detailed SPPCC.

where V_{dc} is the dc bus voltage of the inverter, and λ is the adjusting factor tuned by hand.

The proposed SPPCC is used to track the current in the fast model. By using the forward Euler approximation for sampling interval T_f, the fast model (28) is predicted with the following discrete-time equations:

$$x_{2f}(i+1) = A_f x_{2f}(i)d\nu + B_f u_f(i)d\nu + x_{2f}(i) \tag{33}$$

where $v_{qf} = v_q - v_{qs}$ and $v_{df} = v_d - v_{ds}$.

The cost function is shown as follows:

$$J = |i_q^*(i+1) - i_{qf}(i+1)| + |i_d^*(i+1) - i_{df}(i+1)|. \tag{34}$$

IV. Simulation Studies and Experimental Results

A. Simulation

The proposed SPPCC of the PMSM is developed and validated in MATLAB/Simulation software. A designed speed loop is implemented in the subsystem to generate the internal loop's reference i_q^*. The SPPCC algorithm with the quasi-steady state calculation is expressed in the MATLAB function. The speed and current needed are sampled in discrete time directly. The output of a two-level voltage source inverter is a centralized PWM pulse.

Due to its many benefits, including a fixed structure, well-developed tuning criteria, and ease of implementation, the PI controller has maintained a prominent position in the field of control engineering practice. It has been extensively used for driver design. The conventional finite control set MPCC with PI controllers has been proven to have a better dynamic performance than common FOC with PI in much research [33], [34], [35]. Therefore, in this part, the dynamic performance of the SPPCC is compared with the conventional MPCC. The long prediction horizon GPC has advantages, such as good dynamic performance and disturbance rejection [14], [36]. In contrast to other types of MPC, GPC possesses the intrinsic ability to effectively mitigate the impact of dc bias resulting from parameter mismatch, thereby presenting a notable advantage. So, a strategy of GPC as speed controller and MPCC as current controller is also proposed as a comparable experiment. To better understand the dynamic and steady characteristics, the simulation comparisons are comprehensively presented in Fig. 4.

First, the simulations of the SPPCC algorithm, conventional MPCC, and long prediction horizon GPC are described, and the results for the PMSM are depicted. The feedback q-axis current is limited to twice the rated current with 145 A in three methods when a speed reference of 600 r/min is provided at startup. The feedback stator phase current I_{abc} can immediately return to zero in the SPPCC when the rotor speed is close to the reference speed. It allows no rotor speed overshoot for SPPCC and GPC as the rotor arrives at 600 r/min. However, it appears that the noticeable overshoot is 32 r/min for the conventional MPCC in Fig. 4(b). It can be seen from the simulation in Fig. 4(a) that the setting time for the SPPCC with 0.536 s is much shorter than GPC with 0.6 s in Fig. 4(c) and conventional MPCC with 0.836 s. The sudden torque of 153 Nm is given at $t = 0.8$ s and is canceled at $t = 1.2$ s. From the speed ω_r zoom in and torque load T_L of Fig. 4(b), the conventional MPCC shows that the speed recovery time is over 0.2 s. The speed for the SPPCC varies relatively little in Fig. 4(a), because the torque observer can estimate the load accurately in the SPPCC algorithm. Improved predictive control based on the two-time scale of the singular perturbation theory is shown to be the reason for the better performance.

TABLE I
Parameters of the SPMSM

Parameter	Value
Nominal power P_{nom}	28.26 kW
Nominal current $\lvert i_{s,\,nom}\rvert$	55.79 A
Power factor $\cos(\varphi)$	0.82
Nominal speed ω_{nom}	1000 r/min
Number of pole pairs p	4
Stator resistance R	0.169 Ω
Inductance L	7.07 mH
Inertia of SPMSM and load machine J	4.86 kg·m^2
Viscous damping B_v	0.33 N·ms

B. Implementation Platform

Fig. 5 depicts the trials conducted on the machine test bench to validate the proposed method. The SPMSM are powered by a two-level voltage source inverter and controlled by the MPC algorithm. The SPMSM parameters are presented in Table I. The inverter is based on the dual-core TMS320F28379D, which is capable of signal processing at 200 MHz per core. In addition, the 32-bit floating-point DSP features 12-bit mode A/D converters and pulsewidth modulation channels. The control approach is encoded in the C language as an algorithm. The drive comprises three Infineon IGBT4-FF600R12KE4, 1200 V modules. Three hall sensors are employed to measure the current, while one pole-pair rotating resolver from Tamagawa is used to immediately acquire a high positional resolution. The interrupt program is modified so that the vector voltage candidate can be output promptly and executed with a sample time of $T_s = 100$ μs and $T_f = T_s/10$. The speed and current control frequency for all three methods are 1 and 10 kHz, respectively. Both the slow model's predictive horizon P_s and the fast model's predictive horizon P_f are 1 for the SPPCC. In order to validate the effectiveness of the proposed SPPCC algorithm, the conventional MPCC and long prediction horizon GPC are chosen to compare and contrast different situations. In the experiments, the weight factor of the speed GPC is set as $\lambda_c = 1$, and the prediction

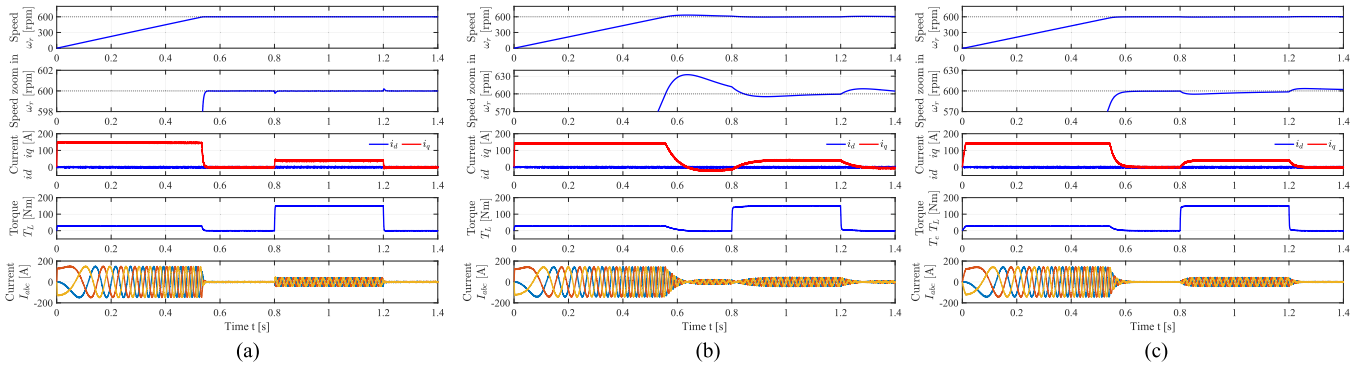

Fig. 4. Simulation response of the PMSM drive to step speed and load torque. (a) Proposed SPPCC. (b) Conventional PI + MPCC. (c) Long prediction horizon GPC.

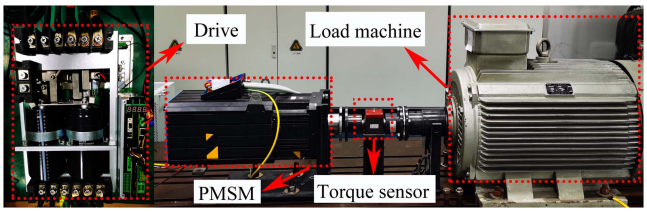

Fig. 5. Test bench utilized to validate the proposed method.

TABLE II
CALCULATION TIME

Methods	Running period	Running time
proposed SPPCC	7 717	38.585 μs
cascaded PI + MPCC	7 181	35.905 μs
long prediction horizon GPC	15 341	76.705 μs

horizon of the speed GPC is set as $N = 90$. The PI parameters of the conventional MPCC are $k_p = 30$ and $k_i = 20$, respectively.

C. Experimental Results

1) Computational Time: The total calculation time among the three methods are listed in Table II. The running period of GPC is much more than the proposed SPPCC and MPCC, because of the calculation burden of long prediction horizon. Herein, the calculation time for the other MPDSC is also challenging. The difference of 2.68 μs between the SPPCC and MPCC algorithms does not affect the control performance significantly for the 100 μs control period. Then, the different test cases are considered for the three methods.

2) Dynamic Performance: In the first test, a large-scale ranges step speed reference from standstill to 600 r/min at $t = 1.39$ s is applied to the PMSM drive on the test bench in Fig. 6. The slight speed of the proposed SPPCC and GPC overshoot is 12 r/min. However, the noticeable overshoot of the conventional method is 42.7 r/min from the speed zoom in of Fig. 6(a). Meanwhile, the setting time with 684 ms of the proposed SPPCC is much shorter than the conventional MPCC with 2 502 ms and GPC with 822 ms. The electromagnetic torque remains approximately twice the rated torque during the rising

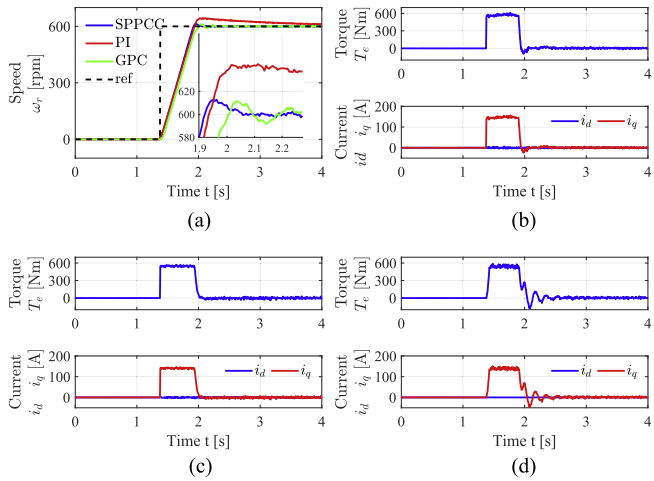

Fig. 6. Large-range step speed. (a) Dynamic speed behavior. (b) Proposed SPPCC. (c) Conventional PI + MPCC. (d) Long prediction horizon GPC.

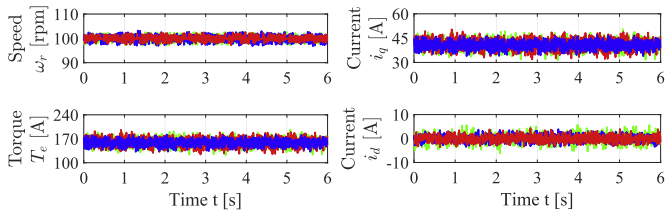

Fig. 7. Steady-state operation with 100 r/min under 153 Nm load (blue—SPPCC, red—PI + MPCC, and green—GPC).

period. But when the actual speed is close to the reference value, the q-axis current of the proposed SPPCC drops dramatically to maintain the precise speed due to predictive sequence values based on the singular perturbation model.

3) Steady-State Performance: The second test is conducted at steady-state operation with 10% rated speed under a 153-Nm torque load and 20% rated speed under a 170-Nm torque load. The results of the three methods shown in Figs. 7 and 8 demonstrate that all methods' speed is stable, and the electromagnetic torque coincides with the actual load torque. Tables III and IV

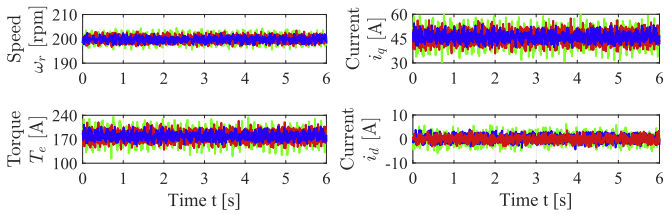

Fig. 8. Steady-state operation with 200 r/min under 170-Nm load (blue—SPPCC, red—PI + MPCC, green—GPC).

TABLE III
SWITCHING FREQUENCIES WITH 100 R/MIN UNDER 153 NM LOAD

Methods	1s	2s	3s	4s	5s	6s
SPCCC	2 238	2 294	2 305	2 280	2 252	2 293
PI + MPCC	5 310	5 339	5 318	5 334	5 290	5 253
GPC + MPCC	3 894	3 978	4 005	3 994	4 015	3 972

TABLE IV
SWITCHING FREQUENCIES WITH 200 R/MIN UNDER 170-NM LOAD

Methods	1s	2s	3s	4s	5s	6s
SPCCC	6 095	6 042	5 930	5 889	5 970	5 885
PI + MPCC	5 154	5 026	5 268	5 269	5 213	5 157
GPC + MPCC	3 436	3 569	3 848	3 783	3 837	3 744

show the corresponding switching frequencies analysis results of three methods. All three methods' dq-axes current correctly tracks the reference without vibration. However, long prediction horizon GPC has significant fluctuation with 4.2 r/min in speed and burrs with 15.2 A in the q-axis current in Fig. 8. There is a slight fluctuation of 3.5 r/min in the certainty speed scope for the conventional MPCC compared with 2.4 r/min for the proposed SPPCC. The number of waveform periods analyzed is 3. The total harmonic distortion (THD) performance of the proposed SPPCC is 1.6% and 3.4% smaller than the conventional MPCC, also 2% and 5.4% smaller than the long prediction horizon GPC for different conditions, respectively. The predictive sequence value of the slow model in the proposed SPPCC is utilized at every fast instant, and the coupling information of the proposed predictive control is more plentiful than the conventional method. As a result, the proposed method not only increases the bandwidth of the speed loop but also is helpful to be more precise in calculating the reference current and reducing the current harmonics. In the context of the singular perturbation theory, an analysis of rapid and slow variables within the electric machine was conducted, where speed and current were, respectively, considered fast and slow variables. The proposed methodology, which optimizes the predictive model sequence, adequately accounts for the impact of speed fluctuations on current. Consequently, within the proposed approach, the influence of speed fluctuations on motor current harmonics is minimized, leading to a reduction in current harmonic levels.

4) Torque Load Disturbance: Afterward, the experimental test is performed as a step torque load from no-load to 153 Nm with 600 r/min at $t = 2.15$ s. The torque load returns to the no-load condition at $t = 6.15$ s. The other step torque test is from 70 to 170 Nm with 200 r/min. The measured speed, the reference

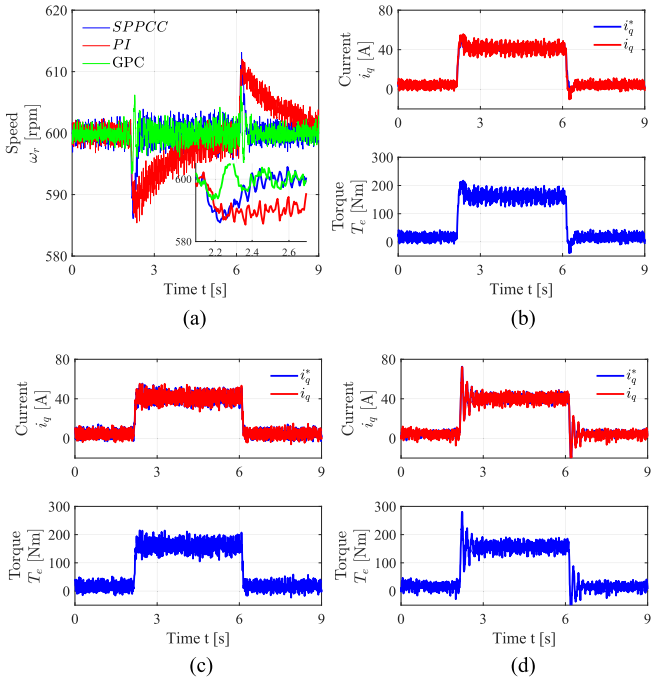

Fig. 9. Load torque change from 0 to 153 Nm, then to 0 Nm. (a) Dynamic speed behavior. (b) Proposed SPPCC. (c) Conventional PI + MPCC. (d) Long prediction horizon GPC.

TABLE V
THD RESULTS

Methods	Fig.7	Fig.8	Fig.10 during step torque process
SPPCC	7.23%	6.52%	12.0%
PI + MPCC	8.89%	9.90%	18.23%
GPC + MPCC	9.24%	11.98%	16.58%

and actual q-axis current, and electromagnetic torque are shown in Figs. 9 and 10. The recovery time of 207 ms of the proposed SPPCC and long prediction horizon GPC is one-fifteenth of the conventional method of 2970 ms in Fig. 9. The SPPCC method's dq-axes current can follow the reference faster. The proposed method can be approximately nearly to the GPC algorithm known as the advantage of disturbance rejection. Furthermore, there is a noticeable current spike of i_q with 72 A at the beginning of sudden torque load in the GPC method. The proposed method, on the contrary, can maintain the appreciable overshoot of i_q with 54 A because of the optimization for prediction sequence with two-time scale of the singular perturbation theory. Table V shows that the THD performance of the proposed SPPCC is 6.2% smaller than the conventional MPCC and 4.6% smaller than the long prediction horizon GPC during the switching state of torque load in Fig. 10.

5) Sensitivity to Parameter's Mismatch: Furthermore, the parameter sensitivity of the SPPCC is investigated because MPC is sensitive to parameter variations easily affected by noise and temperature. The parameter variations are shown in Fig. 11. The test SPMSM runs at steady-state 300 r/min with a 117-Nm torque load in the beginning. At time instant $t = 4.6$ s, R increased by 200% magnitude, and L decreased by 60% magnitude. When

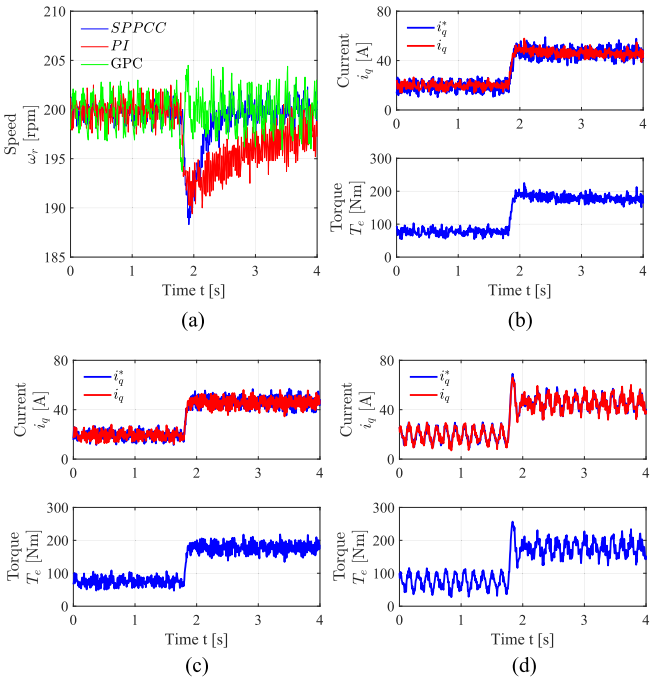

Fig. 10. Load torque change from 70 to 170 Nm. (a) Dynamic speed behavior. (b) Proposed SPPCC. (c) Conventional PI + MPCC. (d) Long prediction horizon GPC.

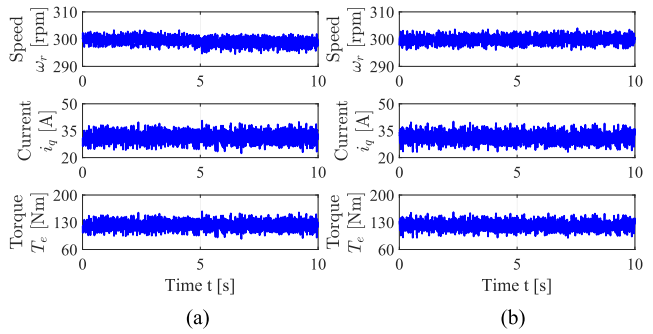

Fig. 11. Parameter sensitive test of the SPPCC. (a) Increased 200% R. (b) Decreased 60% L.

R is increased, the machine's speed maintains the steady-speed control. When L is decreased, the machine speed decreases a little to 297 r/min. Nevertheless, the proposed control system can also correctly track the reference command after a transient response.

The other experimental test about parameter sensitivity is torque load disturbance from 70 to 170 Nm at 400 r/min. In the comparative algorithm, R increased by 200% magnitude, or L decreased by 60% magnitude. Figs. 12 and 13 explicitly indicate that the proposed SPPCC still inherits the strong torque disturbance rejection capability when the critical parameter of the electrical machine is changed. The test results show that the dynamic performance is influenced by inductance parameter variation. The proposed SPPCC has the best current performance with 5-A ripples. However, the noticeable overshoot of i_q with 71 A and current ripples with 13 A are observed for the GPC

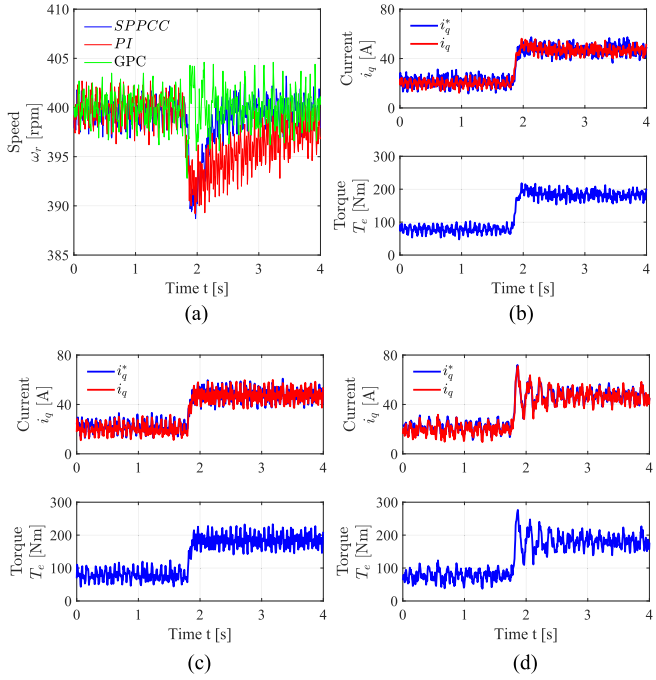

Fig. 12. Inductance sensitive test for torque load change from 70 to 170 Nm. (a) Dynamic speed behavior. (b) Proposed SPPCC. (c) Conventional PI + MPCC. (d) Long prediction horizon GPC.

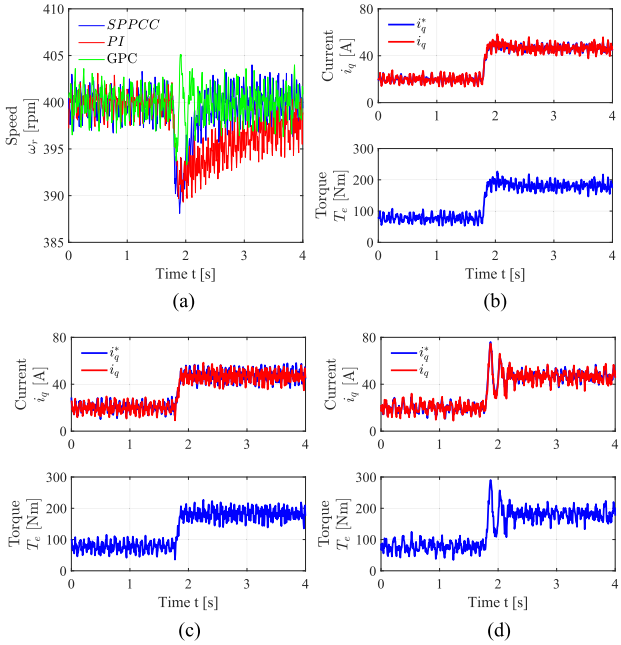

Fig. 13. Resistance sensitive test for torque load change from 70 to 170 Nm. (a) Dynamic speed behavior. (b) Proposed SPPCC. (c) Conventional PI + MPCC. (d) Long prediction horizon GPC.

method in Fig. 12. Fortunately, the proposed SPPCC method still has reduced current ripples and harmonics at different mismatch ratios, as shown in Figs. 12 and 13. The reason is that the singular perturbation can improve the robustness performance when $\epsilon = L/R$ becomes smaller. In the framework of the singular perturbation theory, the slow model is typically regarded

as the primary dynamic behavior of the machine, while the fast model is considered a disturbance. Owing to the primary focus on the slow model, the machine's robustness is generally insensitive to parameter perturbations ϵ occurring in the fast model. This implies that the machine can maintain stability and performance to a significant extent under certain degrees of parameter variation, thus endowing it with a strong degree of robustness.

V. Conclusion

The standard singular perturbation theory is utilized to induce the quasi-steady state and boundary-layer models for the PMSM. The MPC based on the two-time scale characteristic is then described in detail. Then, an enhanced MPC algorithm for speed and current control is evaluated and examined in this article. Experimentally, the proposed strategy has been implemented on a 28-kW prototype test bench. Furthermore, the control system's steady and transient performances are found to be superior to the conventional method PI + MPCC and long prediction horizon method GPC. The test findings also confirm that the strategy is robust to disturbance torque and parameter sensitivity. The two-time scale characteristic of the enhanced MPC algorithm, which makes full use of the singular perturbation theory, is the most crucial feature of this article. Improving the system's dynamics can be helpful in the field of industrial applications. The future work includes developing further voltage antisaturation algorithms to reduce the current oscillation during the saturation of v_{qs} and extending the proposed method to the interior PMSM.

References

[1] H. Lin, S. Niu, Z. Xue, and S. Wang, "A simplified virtual-vector-based model predictive control technique with a control factor for three-phase SPMSM drives," *IEEE Trans. Power Electron.*, vol. 38, no. 6, pp. 7546–7557, Jun. 2023.

[2] P. Karamanakos, E. Liegmann, T. Geyer, and R. Kennel, "Model predictive control of power electronic systems: Methods, results, and challenges," *IEEE Open J. Ind. Appl.*, vol. 1, pp. 95–114, Aug. 28, 2020.

[3] A. Ammar, A. Kheldoun, B. Metidji, B. Talbi, T. Ameid, and Y. Azzoug, "An experimental assessment of direct torque control and model predictive control methods for induction machine drive," in *Proc. Int. Conf. Elect. Sci. Technol. Maghreb*, 2018, pp. 1–6.

[4] Z. Zheng, D. Sun, M. Wang, and H. Nian, "A dual two-vector-based model predictive flux control with field-weakening operation for OW-PMSM drives," *IEEE Trans. Power Electron.*, vol. 36, no. 2, pp. 2191–2200, Feb. 2021.

[5] J. Rodriguez et al., "Latest advances of model predictive control in electrical drives–part I: Basic concepts and advanced strategies," *IEEE Trans. Power Electron.*, vol. 37, no. 4, pp. 3927–3942, Apr. 2022.

[6] J. Rodriguez et al., "Latest advances of model predictive control in electrical drives—Part II: Applications and benchmarking with classical control methods," *IEEE Trans. Power Electron.*, vol. 37, no. 5, pp. 5047–5061, May 2022.

[7] F. Wang, L. He, J. Kang, R. Kennel, and J. Rodríguez, "Adaptive model predictive current control for PMLSM drive system," *IEEE Trans. Ind. Electron.*, vol. 70, no. 4, pp. 3493–3502, Apr. 2023.

[8] Z. Sun, S. Xu, G. Ren, C. Yao, and G. Ma, "A cascaded band based model predictive current control for PMSM drives," *IEEE Trans. Ind. Electron.*, vol. 70, no. 4, pp. 3503–3514, Apr. 2023.

[9] Q. Li, Y. Lv, R. Kennel, and J. Rodriguez, "Model predictive control of PMSM with computed torque for servo press," in *Proc. IEEE Int. Conf. Predictive Control Elect. Drives Power Electron.*, 2023, pp. 1–7.

[10] C. Ma, J. Rodriguez, C. Garcia, and F. De Belie, "Integration of reference current slope based model-free predictive control in modulated PMSM drives," *IEEE Trans. Emerg. Sel. Topics Power Electron.*, vol. 11, no. 2, pp. 1407–1421, Apr. 2023.

[11] T. Wang, G. Luo, C. Liu, Z. Chen, and W. Tu, "Speed control for variable speed PMSM drive system using nonlinear variable-horizon predictive functional control," *IEEE Trans. Emerg. Sel. Topics Power Electron.*, vol. 11, no. 2, pp. 1454–1465, Apr. 2023.

[12] H. Kawai, Z. Zhang, R. Kennel, and S. Doki, "Direct speed control based on finite control set model predictive control with voltage smoother," *IEEE Trans. Ind. Electron.*, vol. 70, no. 3, pp. 2363–2372, Mar. 2023.

[13] S. Wendel, B. Haucke-Korber, A. Dietz, and R. Kennel, "Experimental evaluation of cascaded continuous and finite set model predictive speed control for electrical drives," in *Proc. 21st Eur. Conf. Power Electron. Appl.*, 2019, pp. P–1.

[14] T. Wang, Z.-Q. Zhu, N. M. A. Freire, Z. Wu, M. Foster, and D. A. Stone, "Study on noise and disturbance issues of generalized predictive speed control for permanent magnet synchronous machines," *IET Electric Power Appl.*, vol. 15, no. 1, pp. 63–78, 2020.

[15] F. Karau and M. Leuer, "Model predictive velocity control of electrical drives on an industrial-PC," in *Proc. Int. Symp. Power Electron. Elect. Drives Automat. Motion*, 2022, pp. 76–81.

[16] O. Wallscheid, E. F. B. Ngoumtsa, and J. Böcker, "Hierarchical model predictive speed and current control of an induction machine drive with moving-horizon load torque estimator," in *Proc. IEEE Int. Electric Mach. Drives Conf.*, 2019, pp. 2188–2195.

[17] N. Jabbour and C. Mademlis, "Online parameters estimation and auto-tuning of a discrete-time model predictive speed controller for induction motor drives," *IEEE Trans. Power Electron.*, vol. 34, no. 2, pp. 1548–1559, Feb. 2019.

[18] J. Yang, H. Wu, L. Hu, and S. Li, "Robust predictive speed regulation of converter-driven dc motors via a discrete-time reduced-order GPIO," *IEEE Trans. Ind. Electron.*, vol. 66, no. 10, pp. 7893–7903, Oct. 2019.

[19] X. Zhang and Y. He, "Direct voltage-selection based model predictive direct speed control for PMSM drives without weighting factor," *IEEE Trans. Power Electron.*, vol. 34, no. 8, pp. 7838–7851, Aug. 2019.

[20] C. Lobry and T. Sari, "Singular perturbation methods in control theory," *Contrôle Non Linéaire et Appl.*, vol. 64, pp. 155–182, 2005.

[21] H. Khalil, *Nonlinear Control (Always Learning)*. London, U.K.: Pearson Education Limited, 2014. [Online]. Available: https://books.google.de/books?id=-WbjoAEACAAJ

[22] D. R. Smith, *Singular-Perturbation Theory: An Introduction With Applications*. Cambridge, U.K.: Cambridge Univ. Press, 1985.

[23] R. S. Johnson, *Singular Perturbation Theory: Mathematical and Analytical Techniques With Applications to Engineering*. Berlin, Germany: Springer, 2005.

[24] Z. Zhao et al., "Reduced-order model for wind-solar multi-microgrids considering time-scale coupling," *IEEE Trans. Power Syst.*, to be published, doi: 10.1109/TPWRS.2023.3270366.

[25] M. C. Merchán-Riveros and C. Albea, "Three time-scale singular perturbation hybrid control and large-signal analysis stability in AC-microgrids," *IEEE Trans. Circuits Syst. I, Reg. Papers*, vol. 70, no. 8, pp. 3373–3386, Aug. 2023.

[26] R. Mallik, B. Majmunović, S. Dutta, G.-S. Seo, D. Maksimović, and B. Johnson, "Control design of series-connected PV-powered grid-forming converters via singular perturbation," *IEEE Trans. Power Electron*, vol. 38, no. 4, pp. 4306–4322, Apr. 2023.

[27] P. Li and G. Duan, "High-order fully actuated control approaches of flexible servo systems based on singular perturbation theory," *IEEE/ASME Trans. Mechatronics*, vol. 28, no. 6, pp. 3386–3397, Dec. 2023.

[28] R. F. A. Khan, K. Rsetam, Z. Cao, and Z. Man, "Singular perturbation-based adaptive integral sliding mode control for flexible joint robots," *IEEE Trans. Ind. Electron.*, vol. 70, no. 10, pp. 10 516–10 525, Oct. 2023.

[29] M. Tian, B. Wang, Y. Yu, Q. Dong, and D. Xu, "Robust adaptive resonant controller for PMSM speed regulation considering uncertain periodic and aperiodic disturbances," *IEEE Trans. Ind. Electron.*, vol. 70, no. 4, pp. 3362–3372, Apr. 2023.

[30] M. Tian, B. Wang, Y. Yu, Q. Dong, and D. Xu, "Adaptive active disturbance rejection control for uncertain current ripples suppression of PMSM drives," *IEEE Trans. Ind. Electron.*, vol. 71, no. 3, pp. 2320–2331, Mar. 2024.

[31] J. Zhao, C. Yang, W. Gao, and L. Zhou, "Reinforcement learning and optimal control of PMSM speed servo system," *IEEE Trans. Ind. Electron.*, vol. 70, no. 8, pp. 8305–8313, Aug. 2023.

[32] S. Li and Z. Liu, "Adaptive speed control for permanent-magnet synchronous motor system with variations of load inertia," *IEEE Trans. Ind. Electron.*, vol. 56, no. 8, pp. 3050–3059, Aug. 2009.
[33] X. Zhang, L. Zhang, and Y. Zhang, "Model predictive current control for PMSM drives with parameter robustness improvement," *IEEE Trans. Power Electron.*, vol. 34, no. 2, pp. 1645–1657, Feb. 2019.
[34] A. A. Ahmed, "Fast-speed drives for permanent magnet synchronous motor based on model predictive control," in *Proc. IEEE Veh. Power Propulsion Conf.*, 2015, pp. 1–6.
[35] F. Wang, S. Li, X. Mei, W. Xie, J. Rodríguez, and R. M. Kennel, "Model-based predictive direct control strategies for electrical drives: An experimental evaluation of PTC and PCC methods," *IEEE Trans. Ind. Inform.*, vol. 11, no. 3, pp. 671–681, Jun. 2015.
[36] Q. Li, Q. Chen, J. Gao, A. Li, H. Li, and R. Kennel, "Application of hybrid model predictive control for servo press," in *Proc. IEEE Int. Conf. Predictive Control Elect. Drives Power Electron.*, 2021, pp. 426–431.

Qi Li was born in Shandong, China, in 1986. He received the B.E. degree from Qingdao University, Qingdao, China, in 2008, and the M.E. degree from the Beijing University of Technology, Beijing, China, in 2011, both in automation engineering. He is currently working toward the Ph.D. degree in electrical drive with the Institute for High-Power Converter Systems, Technical University of Munich, Munich, Germany.

From 2011 to 2018, he worked as an Engineer to develop electrical drives for electric vehicles, construction machinery, and servo motors in China. His research interests include electrical drives, predictive control, nonlinear control, and servo press.

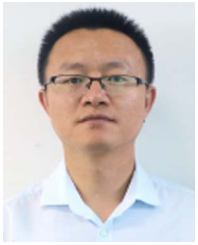

Haiming Li was born in Sichuan, China, in 1981. He received the B.E. degree from University of Electronic Science and Technology of China, Chengdu, China, in 2004, and the M.E. degree from Shandong University, Jinan, China, in 2004, both in electrical engineering.

From 2004 till now, he worked as an Electrical Engineer, Deputy General Manager, and General Manager with Jining Keli Photoelectronic Industrial Company Ltd., Jining, China. His research interests include electrical drives, photoelectronic sensor, and laser radar.

Jianbo Gao received the bachelor's, M.S., and Dr.-Ing. degrees from Tsinghua University, Beijing, China, in 1994, 1997, and 2001, respectively.

From 2001 to 2008, he was a Scientific Coworker and the Head of Chinese Department, Fraunhofer Institute for Biomedical Engineering, Germany. From 2010 to 2013, he was a Postdoctoral Fellow with the Department of Electronics and Information, Technical University Munich, Germany. From 2008 to 2009 and from 2014 to 2016, he was an Engineer and the Head Engineer with his working company in Germany. Since 2017, he has been a Researcher and Team Leader with the Shandong Academy of Sciences, Jining, China. His research interests include power electronics, motion control, intelligent machinery, and their industrial applications.

Ralph Kennel (Life Senior Member, IEEE) was born in Kaiserslautern, Germany, in 1955. He received the diploma and Dr.-Ing. (Ph.D.) degrees in electrical engineering from the University of Kaiserslautern, Kaiserslautern, in 1979 and 1984, respectively, and the doctoral degree honoris causa from Universitatea Stefan cel Mare, Suceava, Romania, in 2018.

From 1983 to 1999, he worked on several positions with Robert BOSCH GmbH (Germany). Until 1997, he was responsible for the development of servo drives. He was one of the main supporters of VECON and SERCOS interface, two multicompany development projects for a microcontroller and a digital interface especially dedicated to servo drives. Furthermore, he took an active part in the definition and release of new standards with respect to CE marking for servo drives. Between 1997 and 1999, he was responsible for Advanced and Product Development of Fractional Horsepower Motors in automotive applications. His main activity was preparing the introduction of brushless drive concepts to the automotive market. From 1994 to 1999, he was an appointed Visiting Professor with the University of Newcastle-upon-Tyne, Newcastle upon Tyne, U.K. From 1999 to 2008, he was a Professor for electrical machines and drives with Wuppertal University, Germany. Since 2008, he has been a Professor for electrical drive systems and power electronics with Technische Universitaet Muenchen, Munich, Germany. He was an appointed Extraordinary Professor with the University of Stellenbosch, South Africa, from 2016 to 2019, and as a Visiting Professor with the Haixi Institute, Chinese Academy of Sciences, Fuzhou, China, from 2016 to 2021. His main interests include sensorless control of ac drives, predictive control of power electronics, and hardware-in-the-loop systems.

Dr. Kennel is a Fellow of IET (former IEE) and a Chartered Engineer in the U.K. Within IEEE, he is Treasurer of the Germany Section as well as Distinguished Lecturer of the Power Electronics Society (IEEE-PELS). He was the recipient of the 2013 Harry Owen Distinguished Service Award from IEEE-PELS, the EPE Association Distinguished Service Award in 2015, as well as the 2019 EPE Outstanding Achievement Award.